IEEE Access
Multidisciplinary ⋮ Rapid Review ⋮ Open Access Journal

Received 26 April 2024, accepted 19 May 2024, date of publication 23 May 2024, date of current version 3 June 2024.

Digital Object Identifier 10.1109/ACCESS.2024.3404641

RESEARCH ARTICLE

Parameters Estimation of Proton Exchange Membrane Fuel Cell Model Based on an Improved Walrus Optimization Algorithm

AYEDH H. ALQAHTANI[1], (Senior Member, IEEE), HANY M. HASANIEN[2,3], (Senior Member, IEEE), MOHAMMED ALHARBI[4], AND SUN CHUANYU[5], (Member, IEEE)

[1]Electrical Engineering Department, College of Technological Studies, The Public Authority for Applied Education and Training, Safat 23167, Kuwait
[2]Electrical Power and Machines Department, Faculty of Engineering, Ain Shams University, Cairo 11517, Egypt
[3]Faculty of Engineering and Technology, Future University in Egypt, Cairo 11835, Egypt
[4]Electrical Engineering Department, College of Engineering, King Saud University, Riyadh 11421, Saudi Arabia
[5]School of Electrical Engineering and Automation, Harbin Institute of Technology, Harbin 150006, China

Corresponding author: Hany M. Hasanien (hanyhasanien@ieee.org)

This work was supported by King Saud University, Riyadh, Saudi Arabia, through the Researchers Supporting Project under Grant RSP2024R467.

ABSTRACT Proton Exchange Membrane Fuel Cells (PEMFCs) play a crucial role in the advancement of clean hydrogen vehicles. Their ability to convert hydrogen into electricity makes them promising candidates to replace conventional engines. However, optimizing their performance and efficiency necessitates accurate modeling techniques capable of simulating their behavior. In this context, this paper proposes an advanced approach for precise parameter estimation in PEMFC models. Employing an Enhanced Walrus Optimization (EWO) algorithm integrated with Lévy flight exploration, the approach tackles the inherent nonlinearity of PEMFC systems. The technique aims to minimize the squared error between measured and simulated terminal voltage, thereby ensuring superior accuracy and robustness compared to established algorithms. The effectiveness of the proposed model is validated through comparisons between theoretical simulations and experimental measurements. The findings demonstrate the efficacy of the EWO algorithm, consistently outperforming previously published algorithms and achieving notably lower errors. Moreover, the incorporation of Lévy flights enhances the algorithm's capabilities, leading to expedited convergence and more accurate parameter estimations. Beyond facilitating precise parameter estimation, this enhanced modeling strategy opens avenues for refining design and optimization strategies in fuel cell research and development. The major contributions of this paper include the enhancement of the WO algorithm, evaluation of theoretical model accuracy, and robustness assessment of the EWO in optimizing the PEMFC model. By furnishing accurate models validated through experimental evidence, this enhanced modeling strategy paves the way for refining design and optimization strategies in fuel cell research and development.

INDEX TERMS Accurate modeling, artificial intelligence, optimization methods, parameter estimation, PEM fuel cells.

I. INTRODUCTION

A. PROBLEM UNDER STUDY

The limited characteristics and ecological ramifications of fossil fuels mandate a transition towards environmentally friendly energy alternatives [1]. Fuel cells, which convert chemical energy into electricity through electrochemical reactions, emerge as promising candidates in this endeavor [2]. In terms of clean energy technologies, fuel cells stand out due to their outstanding efficiency and emission-free power generation capabilities [2], [3]. Unlike conventional power generators, fuel cells produce energy

The associate editor coordinating the review of this manuscript and approving it for publication was Lei Wang.

through the electrochemical reaction of hydrogen and oxygen [4], [5]. This clean process significantly reduces the environmental impact, particularly in terms of greenhouse gas emissions and air pollution [6]. Proton exchange membrane fuel cells (PEMFCs) [7], solid oxide fuel cells (SOFCs) [8], and molten carbonate fuel cells (MCFCs) [9] are three distinct types of fuel cells that find application in various domains. SOFCs, known for their versatility in fuel usage and ability to operate at higher temperatures, are well-suited for stationary power generation [10]. Furthermore, the modular design of fuel cells allows for scalability, accommodating both compact, portable devices and large-scale power plants [11]. As such, fuel cells present a viable option for various applications, including residential, commercial, and industrial energy supply [12].

PEMFCs have gained recognition for their remarkable efficiency and minimal emissions [13]. The focus of this study centers on the precise modeling of PEMFCs, with the goal of paving the way for optimized design strategies that contribute to a cleaner and more sustainable future. In the midst of the global transition towards cleaner energy sources, PEMFCs play a crucial role in reducing reliance on fossil fuels, curbing pollution, and ensuring energy security [14]. Their growing prominence in sectors such as transportation [15], distributed generation, and microgrids underlines the importance of this research, which explores the field of these clean energy options and future advancements in fuel cell technology [16]. The construction of accurate models for PEMFCs has become a pivotal point for researchers [17] who seek to establish reliable models using software programs that closely correlate with experimental results [18]. The significance of PEMFC modeling lies in its impact on analyses, particularly in microgrids and smart grid applications [19].

B. LITERATURE REVIEW

Various modeling approaches are employed [20], [21], encompassing analytical, empirical, semi-empirical, and theoretical methods to simulate PEMFC performance [22]. Theoretical extraction of PEMFC parameters involves both conventional and metaheuristic methods [23]. Reference [24] focuses on PEMFC parameter estimation, highlighting the challenges posed by nonlinear systems for accurate modeling. The review emphasizes the use of empirical equations for design purposes. The contribution of this reference is: (1) reviews existing methods, (2) introduces novel techniques like neural networks and bio-inspired algorithms, (3) aims to aid researchers in developing even better estimation techniques. The drawbacks mentioned in that reference are: (1) GA has weak exploitation capability, (2) Harmony Search Algorithm (HSA) suffers from premature convergence. Reference [25] presents two novel iterative techniques for solving a critical nonlinear equation in PEMFC modeling, along with a hybrid optimization algorithm that outperforms existing methods in estimating PEMFC parameters for enhanced model accuracy. In [26], a semi-empirical PEMFC model is implemented using novel grey wolf optimization algorithm. This methodology is tailored to capture the dynamic behavior of PEMFCs in real-world conditions, offering advantages over traditional optimization techniques. The study in [27] employs an empirical performance degradation model, assessing the contributions of aging factors to PEMFC power loss by fitting parameters to measured polarization curves. The drawbacks mentioned in this reference are: (1) The physical-based approaches for degradation modeling face challenges, (2) The data-driven approaches rely on experimental data which may lack understanding of degradation states, and (3) Difficulty in predicting accurate lifespan. The study presented in [28] evaluates six optimization techniques on PEMFC models, identifying performance disparities and highlighting the most accurate one supported by MATLAB validations. The limitation in this reference is the high failure rate in production of fuel cells, leading to high costs and low reliability. In [29], three metaheuristic optimization techniques are introduced to determine the parameters of PEMFCs, demonstrating that these methods solve the optimization problem with minimal differences in performance. In [30], a semi-empirical approach is proposed that combines variational Bayes for parameter estimation and Sobol sensitivity analysis for PEMFC modeling, offering a high level of accuracy and reduced computational effort while quantifying parameter sensitivity and uncertainty under varying conditions. The limitations mentioned in this reference are: (1) The complexity of equations in mechanism models leads to long computation times, (2) The data-driven models require a large amount of data and are time-consuming to build. The study in [31] examines the degradation prediction of a PEMFC stack through semi-empirical and data-driven models to forecast long-term stack performance degradation with improved accuracy. The drawbacks mentioned in this reference are: (1) Obtaining test data for the whole life cycle is challenging, (2) The degradation processes of leaking current impact the performance. Reference [32] presents a novel semi-empirical model for PEMFC voltage estimation, optimizing parameters using the lightning search algorithm and validating the model under various conditions. The drawbacks mentioned in this reference are: (1) The semiempirical model for voltage prediction needs correction through experimentation, (2) The parameters in the model vary with ambient conditions, affecting accuracy, and (3) Semiempirical models lack the complexity and accuracy. Reference [33] proposes a new optimization algorithm, Combined Owl Search Algorithm, for estimating optimal parameters in PEMFC fuel cell stacks, achieving lower errors compared to existing methods. A novel Dandelion Optimizer is proposed in [34] to accurately identify the parameters of the PEMFC model, addressing challenges associated with nonlinearity and the unknown parameters, with comparative analysis with existing optimization algorithms. The drawbacks mentioned in this reference are: (1) Metaheuristic optimizers face challenges related to convergence to local minima, (2) Other optimizers have slow convergence

to local optima, and (3) The need for accurate extraction of PEMFC parameters highlights the limitations in modeling and validation of PEMFCs.

C. MAIN CONTRIBUTION

The primary objective of this study is to develop robust and reliable fuel cell models, specifically focusing on PEMFCs. The research endeavors to establish a theoretical model that accurately represents PEMFC behavior, aligning closely with experimental data. This model incorporates seven unknown design variables and effectively captures the nonlinear relationship between current and voltage (I-V). An objective function is employed to minimize the sum of squared errors (SSE), facilitating the determination of optimal values for these variables. Various optimization algorithms shall be used in a study to validate a robust model for the PEMFC such as Remora Optimization Algorithm (ROA), Dynamic Harris Hawks Optimization with Mutation Mechanism (DHHO/M), and Harris Hawks Optimization with Differential Evolution (HHO-DE) [35]. To validate the model's robustness in this study, an Enhanced version of the Walrus optimization (EWO) algorithm is proposed and tested across various pressure and temperature conditions.

The Warlus optimization (WO) algorithm, introduced in 2024 by Muxuan Han et al., is an innovative nature-inspired metaheuristic algorithm. It distinguishes itself by achieving a balance between exploration and exploitation, resulting in rapid convergence and high efficiency. The WO algorithm is applicable to a wide range of optimization challenges. Recognizing its impressive performance, an enhanced version of the WO algorithm is investigated to address the complexities of PEMFC modeling. The objective is to leverage the strengths of the WO algorithm while introducing targeted modifications to improve the accuracy and efficiency of PEMFC parameter extraction. The key contributions of this work can be written as follows:

1) Enhancement of the WO: Developing an improved WO variant, named EWO, which achieves superior performance in optimization tasks.
2) Evaluation of theoretical model accuracy: Assessing the effectiveness of the model by comparing simulated I-V curves with experimental data.
3) Robustness demonstration of the EWO: Validating the algorithm's robustness by comparing its outcomes with those of alternative optimization algorithms and verifying its capability to minimize the objective function.

D. PAPER STRUCTURE

The paper is organized to offer a thorough exploration of the aforementioned topics. Section II outlines the mathematical model of the PEMFC. Following that, Section III covers the formulation of the optimization problem, containing the objective function and constraints. Section IV provides a detailed description of the newly devised and improved optimization algorithm, EWO. Subsequently, Section V presents the simulation outcomes and numerical comparisons with alternative algorithms. Finally, Section VI concludes the paper by summarizing key findings and proposing directions for future research, providing insights into potential advancements and applications.

II. PEMFC MATHEMATICAL MODEL

The mathematical formulation used to describe the PEMFC in our investigation is presented in this section. The PEMFC model selection aligns with the framework outlined in [36], which has demonstrated its efficiency in accurately modeling the cell's behavior and has served as a benchmark in numerous prior research efforts. The terminal voltage (V_{stack}) of the PEMFC is expressed using Equation (1), which takes into consideration the number of series-connected cells (N_{cells}). The total voltage of the stack is the sum of the voltages across each individual cell. Connecting cells in series increases the total output voltage of the stack. This Equation is the fundamental element for subsequent analysis in this work [37].

$$V_{stack}=N_{cells}.\left(E_{nernst}-v_{act}-v_{\Omega}-v_{conc}\right) \tag{1}$$

where E_{nernst} is the Nernst potential which calculates the theoretical voltage of a fuel cell under open-circuit conditions. It is dependent on the temperature and pressure [38]. v_{act} is the activation overpotential. v_{Ω} represents the voltage loss due to the resistance. It is influenced by the conductivity of the materials used in the cell. v_{conc} is the concentration overpotential. Equation (2) calculates the theoretical open-circuit voltage of a PEMFC, E_{nernst} [37].

$$\begin{aligned} E_{Nernst} &= 1.229-0.85\times10^{-3}\left(T_{fc}-298.15\right) \\ &\quad +4.3085\times10^{-5}T_{fc}ln\left(P_{H_2}\sqrt{P}_{O_2}\right) \end{aligned} \tag{2}$$

Here, T_{fc} denotes the temperature of the PEMFC measured in Kelvin. P_{H_2} and P_{O_2} represent the partial pressures of hydrogen and oxygen, respectively. The voltage drops v_{act}, v_{Ω}, and v_{conc} are determined by (3)-(5), respectively.

$$\begin{aligned} v_{act} &= -\left[\xi_1+\xi_2T_{fc}+\xi_3T_{fc}ln\left(C_{O_2}\right)\right. \\ &\quad \left.+\xi_4T_{fc}ln\left(I_{fc}\right)\right] \end{aligned} \tag{3}$$

where $C_{O_2}=\frac{P_{O_2}}{5.08\cdot10^6}\cdot exp\left(498/T_{fc}\right)$

$$v_{\Omega}=I_{fc}\left(R_m+R_c\right);\ R_m=\frac{\rho_m l}{M_A} \tag{4}$$

where ρ_m

$$\begin{aligned} &= \frac{181.6\left[1+0.03\left(\frac{I_{fc}}{M_A}\right)+0.062\left(\frac{I_{fc}}{303}\right)^2\left(\frac{I_{fc}}{M_A}\right)^{2.5}\right]}{\left[\lambda-0.634-3\left(\frac{I_{fc}}{M_A}\right)\right]\cdot exp\left[4.18\left(\frac{T_{fc}-303}{T_{fc}}\right)\right]} \\ v_{conc} &= -\beta\cdot ln\left(1-\frac{J}{J_{max}}\right) \end{aligned} \tag{5}$$

where ξ_1, ξ_2, ξ_3, and ξ_4 are empirical coefficients. C_{O_2} is the concentration of oxygen. I_{fc} is the fuel cell current. R_m and R_c represent the membrane and contact resistances, respectively. ρ_m is the membrane resistivity, which varies with current

density and temperature. l is the thickness of the membrane, and M_A is the membrane surface area. β is an empirical coefficient. J is the current density, and J_{max} is the maximum current density. λ is a design variable that affects various aspects of the fuel cell's performance. It is assumed to be between 13 and 23. β is a design variable from 0.0136 to 0.5.

These equations collectively constitute a comprehensive model for analyzing the performance of PEMFCs, considering various factors that impact cell voltage. The comprehension and optimization of these parameters are essential for enhancing fuel cell efficiency and overall performance. The control parameters (ξ_1, ξ_2, ξ_3, ξ_4, λ, R_c, and β) play a critical role in building a comprehensive and precise model of PEMFC performance. These variables need to be meticulously determined to facilitate the application of this model in power system investigations and the refinement of fuel cell designs for diverse applications. With the mathematical groundwork of the PEMFC model established, Section III outlines the problem formulation, encompassing the objective function, for optimizing the identified design variables.

III. PROBLEM FORMULATION

Due to limited data availability from manufacturers, the PEMFC model incorporates nonlinear characteristics, posing a challenge for accurate modeling [37]. To tackle this obstacle, the optimal values for the control parameters are estimated by minimizing the SSE between the model's predicted voltage and the empirically measured fuel cell voltage [39]. Formulated as a non-convex optimization problem, this minimization task seeks to align the model's predictions closely with the experimental data. The mathematical representation of this objective function is provided in Equation (6) [40]:

$$SSE = \sum_{m=1}^{N_{samples}} \left[V_{FC,exp}(m) - V_{FC,e\ st}(m)\right]^2 \tag{6}$$

where $N_{samples}$ represents the total count of measured voltages. $V_{FC,exp}$ denotes the terminal voltage of the PEMFC as observed in the experiments, expressed in volts (V). $V_{FC,est}$ signifies the terminal voltage of the PEMFC estimated by the model, also in volts (V). In order to ensure that the estimated values remain within practical and realistic ranges, the fitness function incorporates seven design variables. These variables, which are denoted as ξ_1−ξ_4, λ, Rc, as well as β, are subject to both maximum and minimum bounds, which are represented as inequality constraints. Eventually, the ability to reduce the SSE and improve the model's accuracy is facilitated by modifying these variables utilizing the EWO. To accomplish this, the suggested optimization approach employs the MATLAB software. With the objective function established and the design variables identified alongside their constraints, the subsequent section delves into the optimization solution's core, presenting a novel approach that addresses the optimization problem effectively.

IV. EWO ALGORITHM DETAILS

A. STANDARD WALRUS OPTIMIZER ALGORITHM

The WO algorithm is a newly developed metaheuristic algorithm that draws inspiration from the diverse behaviors of walruses in nature. This algorithm simulates the social structures and capabilities exhibited by these marine mammals [41]. Walruses are known for their keen sense of touch, a trait integrated into the WO algorithm through the modeling of populations and their reactions to perceived danger and safety cues. Moreover, it considers the social dynamics and hierarchies within walrus groups, which consist of adults, juveniles, and females. These elements guide the WO's search process, balancing exploration and exploitation effectively. This section elaborates on the core concepts forming the WO algorithm.

Initialization: The WO optimization process commences with an initial population of candidate solutions randomly generated within the predetermined lower and upper bounds established for the optimization problem's design variables. This diverse starting point ensures adequate search space exploration for potential optima. As the WO progresses, the agents are guided by social and environmental cues, allowing them to refine their positions and approach closer to reaching optimal solutions.

Danger and Safety Signals (The Guiding Force of Walrus Behavior): The WO algorithm relies on the idea of ''safety'' and ''danger'' signals, mirroring the responsiveness of walruses to their surroundings. These signals influence the individual behavior of each agent and guide the entire population toward regions likely to contain optimal solutions. The danger signal reflects the risk associated with an agent's current position. It is calculated using Equation (7). This danger signal gradually weakens throughout optimization, encouraging agents to converge towards promising solutions.

On the other hand, the safety signal represents the attractiveness of an agent's current location. It is calculated using Equation (11). This signal increases with each iteration, promoting exploitation. By effectively balancing these opposing forces, the WO algorithm navigates the search space efficiently [41].

$$\text{Danger\_signal} = A \times R \tag{7}$$

$$A = 2 \times \alpha \tag{8}$$

$$\alpha = 1 - \frac{t}{T} \tag{9}$$

$$R = 2 \times r_1 - 1 \tag{10}$$

$$\text{Safety\_signal} = r_2 \tag{11}$$

In the previous equations, A and R signify the risk elements, the parameter α decreases from 1 to 0 across the optimization process. The stochastic variables r_1 and r_2 range between 0 and 1, with r_2 specifically indicating the safety signal. The variable t is used to denote the current iteration step, whereas T represents the maximum predetermined number of iterations.

The Migration stage: The migration stage represents the exploration aspect, where walrus agents attempt to get into new zones of the search space. During this stage, the location of each agent is reorganized based on migration step β, as well as a random number r_3.

The walrus position update equation is as follows [41]:

$$X_{ij}^{t+1} = X_{ij}^{t} + Migration\_step \tag{12}$$

$$Migration\_step = \left(X_m^t - X_n^t\right) \times \beta \times r_3^2 \tag{13}$$

$$\beta = 1 - \frac{1}{1 + e^{\frac{-10(t-0.5T)}{T}}} \tag{14}$$

where X_{ij}^{t+1} represents the updated location in iteration i along dimension j. X_m^t and X_n^t denote two positions chosen at random. Diversifying the Population (Reproduction Stage): This stage models different behaviors for three categories: males, females, and young walruses. Male walruses act as scouts, exploring new regions of the search space. Their positions are redistributed. Female walruses represent exploitation, focusing on refining promising solutions. Young walruses introduce additional diversification. Their positions are updated based on interactions with both parents, incorporating exploration and exploitation elements while adding randomness for further exploration. Through these diverse reproduction strategies, the WO algorithm maintains a balance between exploring new regions and exploiting promising solutions, enhancing its ability to find optimal results. The formulation of this stage can be expressed as shown in Equations (15)-(17) [41]:

$$female_{ij}^{t+1} = female_{ij}^{t} + \alpha \times \left(male_{ij}^{t} - female_{ij}^{t}\right) + (1-\alpha) \times \left(X_{best}^{t} - female_{ij}^{t}\right) \tag{15}$$

$$Juvenile_{ij}^{t+1} = \left(O - Juvenile_{ij}^{t}\right) \times P \tag{16}$$

$$O = X_{best}^{t} + Juvenile_{ij}^{t} \times LF \tag{17}$$

where O denotes the benchmark location for safety, and P corresponds to the risk factor associated with juvenile walruses.

B. ENHANCED WALRUS OPTIMIZATION ALGORITHM

Lévy flight is a movement pattern characterized by sharp changes in direction and long-distance jumps with shorter steps [42]. This stochastic behavior, represented by Lévy distributions, has been shown to significantly improve optimization algorithms [43], [44]. By incorporating Lévy flights, algorithms can more adeptly evade local optima, explore diverse regions successfully, and detect globally optimal solutions. Lévy flights can be integrated into optimization algorithms by adjusting the position updates of candidate solutions. Its effectiveness depends on the precise tuning of parameters such as the distribution's scale and exponent.

The EWO improves upon the original WO by adopting the Lévy flight strategy. This addition allows the algorithm to explore broader areas within the search space, thereby improving the algorithm's efficiency in finding optimal solutions. Including Lévy flights changes how positions are updated within the WO, demonstrating the effectiveness of metaheuristic optimization approaches. Consequently, the EWO reveals enhanced convergence capabilities, positioning it as a powerful tool for problem optimization. The formulation of the Lévy function can be expressed mathematically as shown in Equation (18) [45]:

$$LF = 0.01 \times \frac{u \times \sigma}{|v|^{\frac{1}{\gamma}}}, \sigma = \left(\frac{\Gamma(1+\gamma) \times sin\left(\frac{\pi\gamma}{2}\right)}{\Gamma\left(\frac{1+\gamma}{2}\right) \times \gamma \times 2^{\left(\frac{\gamma-1}{2}\right)}}\right)^{\frac{1}{\gamma}} \tag{18}$$

The parameters u and v, being random variables that range from 0 to 1, introduce variability and randomness into the model. The flowchart in Figure 1 depicts the optimization process using the EWO algorithm.

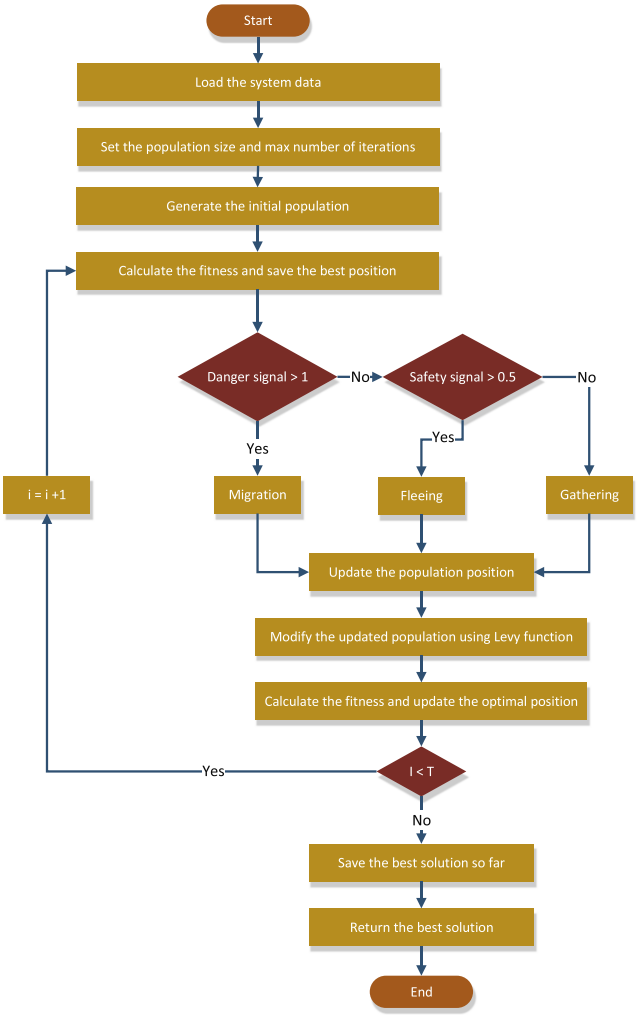

FIGURE 1. Flowchart of the EWO algorithm.

V. SIMULATION RESULTS AND ANALYSIS

A. CASE 1: PERFORMANCE OF 6 kW Nedstack PS6 PEMFC

In this case, the focus is on the Nedstack PS6 PEMFC, whose output power is 6 kW. The analysis of this PEMFC is executed through the utilization of Matlab, with the simulation being conducted at a temperature of 338 K, whilst both

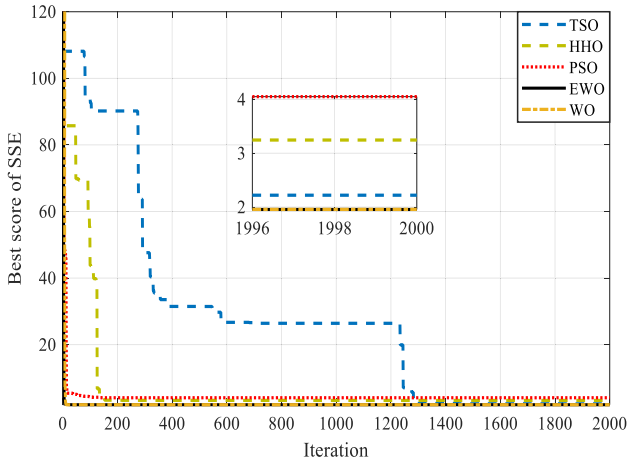

FIGURE 2. Convergence curves for case 1.

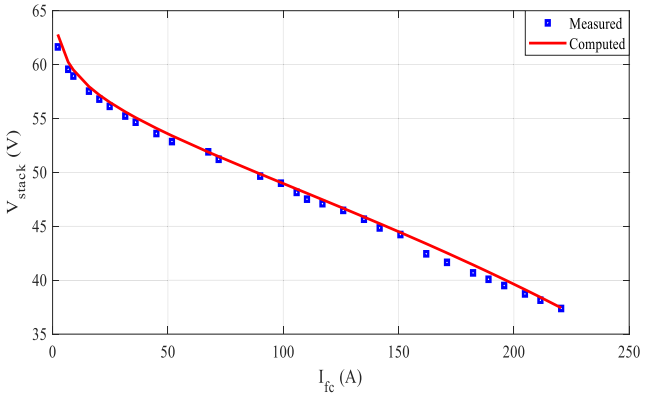

FIGURE 3. I-V curves for case 1.

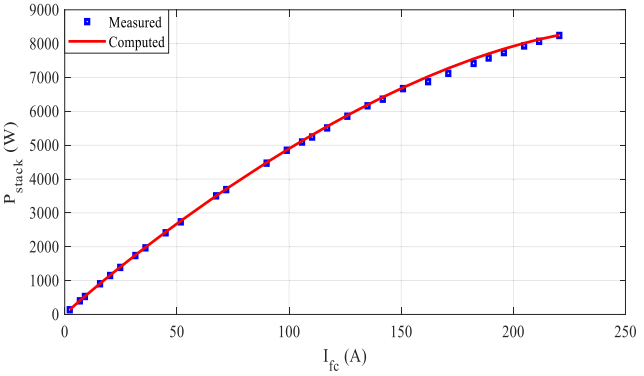

FIGURE 4. I-P curves for case 1.

TABLE 1. Design variables for case 1.

Parameter	EWO	WO	TSO [36]	HHO [40]	PSO [36]
$\xi_1 \times 10^{-1}$	-9.14845	-8.532	-8.532	-8.54040032	-8.532
$\xi_2 \times 10^{-3}$	2.628048	2.41122	2.461745	2.735106	2.604769
$\xi_3 \times 10^{-5}$	3.85401	3.60487	3.94	5.82447	4.89593
$\xi_4 \times 10^{-5}$	-9.54	-9.54	-9.54	-9.54	-9.54
λ	13.01394683	13	14.1357	16.71211946	23
$R_c \times 10^{-3}$	0.1	0.1	0.109423	0.338306	0.139638
β	0.0136	0.0136	0.1139157	0.046842862	0.5
SSE	1.95552479	1.95665988	2.219	3.244844681	4.050851284

oxygen and hydrogen pressures are set at 1 atm. The fuel cell consists of a total of 65 cells that are connected in series. The membrane possesses a thickness measuring 1.78 mm. Another specification is the fuel cell's surface area, which measures 240 cm^2. The maximum current density that the fuel cell can withstand is 5A/cm^2 [37]. Figure 2 illustrates the convergence curves of four different algorithms: transient search optimization (TSO), harris hawk optimization (HHO), particle swarm optimization (PSO), and EWO over a series of 2000 iterations. The graph outlines the optimal score of the fitness function that each algorithm achieved as the iterations progressed. The EWO algorithm demonstrated the highest efficiency, converging to its best score in the fewest iterations. In contrast, TSO exhibited a slower convergence, requiring over 1200 iterations to become stable. The graph also features a subplot that zooms in on the final four iterations, highlighting the advantage of the proposed algorithm.

The analysis of the fuel cell's electrical characteristics is explained through two figures. Figure 3 outlines the I-V characteristics, comparing the computed estimates and 29 individual voltage measurements. The correspondence between the estimated and measured voltage values is marked, indicating a reliable match. Also, Figure 4 exemplifies the correlation between the PEMFC's current and its output power. Similar to the I-V characteristics, this figure compares the estimated power values to measured data points across varying current levels, verifying the accuracy of the computational estimates against practical measurements. Both figures are essential in understanding the performance of the 6 kW Nedstack PS6 fuel cell.

Table 1, in addition, offers a comparative analysis of the newly developed EWO method against other optimization methods, such as the TSO, the HHO, and the PSO. It shows the optimal candidate solutions for various design parameters in the optimization. These solutions represent the optimal outcomes in minimizing the SSE between the calculated and observed terminal voltages of a PEMFC.

Figure 5 displays a plot of internal voltage losses against the current for a 6 kW Nedstack PS6 fuel cell. The x-axis represents the current in amperes, and the y-axis represents the voltage losses in volts. The plot details the different elements of voltage loss. It exhibits that with an increase in current, there is a corresponding increase in both total voltage losses and ohmic losses. Conversely, the concentration and activation losses tend to stay relatively unchanged across the current range presented.

The following two figures are presented to examine the performance characteristics of a 6 kW Nedstack PS6 PEMFC at various temperatures. Figure 6 compares I-V curves for the PEMFC at temperatures of 15, 40, and 60°C. The x-axis

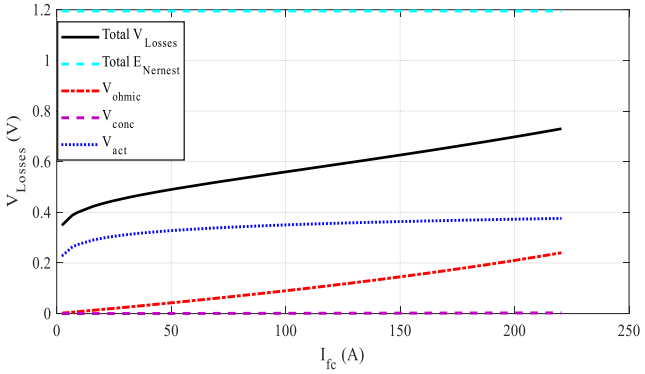

FIGURE 5. Graphical analysis of voltage losses at varying current levels for case 1.

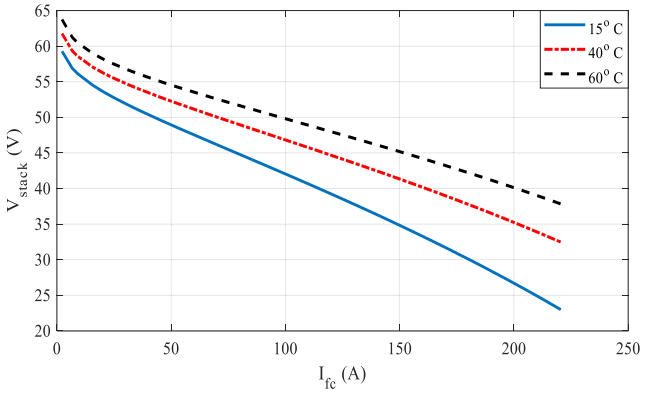

FIGURE 6. I-V curves at various temperatures for case 1.

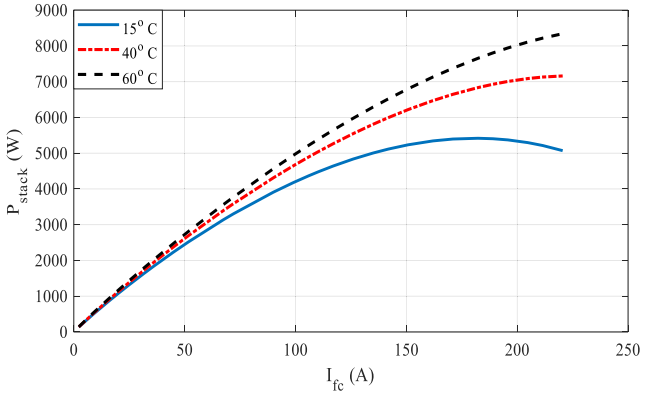

FIGURE 7. I-P curves at various temperatures for case 1.

represents the fuel cell current in amperes, while the y-axis represents the voltage of the stack in volts. The graphs indicate that as the temperature rises, the voltage for a given current also increases. At 60°C, the voltage remains higher across the current range compared to the voltage at 15°C and 40°C. Next, Figure 7 illustrates the comparison of I-P curves under the same temperature conditions. It is evident from the power curves that the output power undergoes minor adjustments with temperature variations. Noticeably, the output power is highest at 60°C and lowest at 15°C.

Following that, the simulations were carried out under different pressures while maintaining a fixed temperature to assess the impact of pressure adjustments on the voltage. The

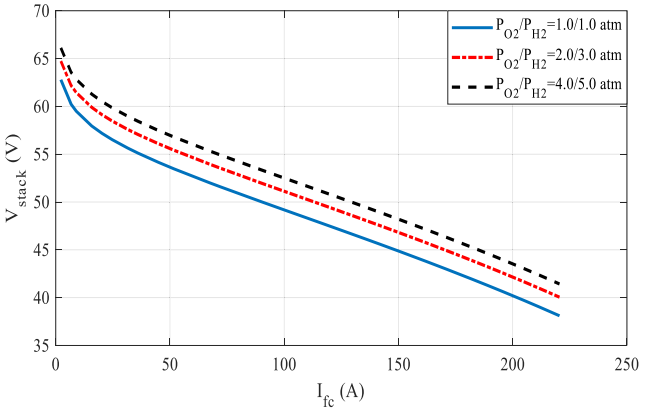

FIGURE 8. I-V curves at various pressures for case 1.

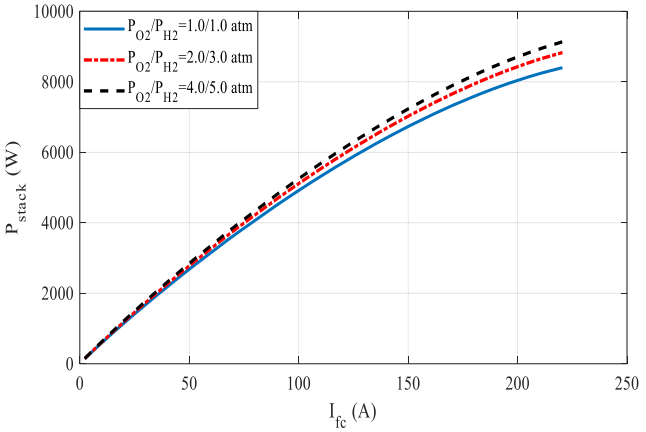

FIGURE 9. I-P curves at various pressures for case 1.

results of these simulations are clearly illustrated in the I-V and I-P graphs depicted in Figures 8 and 9. Analysis of these figures shows a clear increase in voltage with higher pressures. This observation, combined with comparative results obtained from changing temperatures at constant pressure, concludes that temperature variations have a more considerable effect on the fuel cell's voltage and power output than changes in pressure.

B. CASE 2: PERFORMANCE OF 250 W PEMFC STACK

Through the second case, an evaluation is conducted on the performance of a 250 W PEMFC stack, comprising 24 cells in series, in order to optimize it using various algorithms. With an active area of 27 cm^2 in addition to a maximum current density of 860 mA/cm^2, the PEMFC stack shows notable results. The optimization algorithms compared include the mayfly optimization algorithm (MOA), hybrid grey wolf optimizer with circle search (GWO-CS), and the HHO.Table 2lists the best values achieved by the EWO relative to those obtained by the other mentioned algorithms in the literature. The results for the EWO show a lower SSE, indicating more precise optimization.

Figure 10 graphically shows how the SSE decreases over iterations for all the algorithms studied. Importantly, the figure contains a detailed inset of the final five iterations,

TABLE 2. Design variables for case 2.

parameter	EWO	WO	MOA [40]	GWO-CS [40]	HHO [40]
$\xi_1 \times 10^{-1}$	-8.532	-8.53582618	-11.997	-10.4228	-8.9794
$\xi_2 \times 10^{-3}$	2.311002	2.322319	4.22020772	3.105	2.578
$\xi_3 \times 10^{-5}$	3.601	3.85529	9.634	5.56	5.13
$\xi_4 \times 10^{-5}$	-17.489	-1.12594	-17.3535084	-17.274	-11.303
λ	19.93583223	13	19.31880898	21.44088	14.24547
$R_c \times 10^{-3}$	0.1	0.1	0.100000246	0.664	0.506
β	0.01452524	0.0136	0.0136	0.014123	0.014029
SSE	0.335979	1.724021831	0.33718996	0.34040375	1.381575

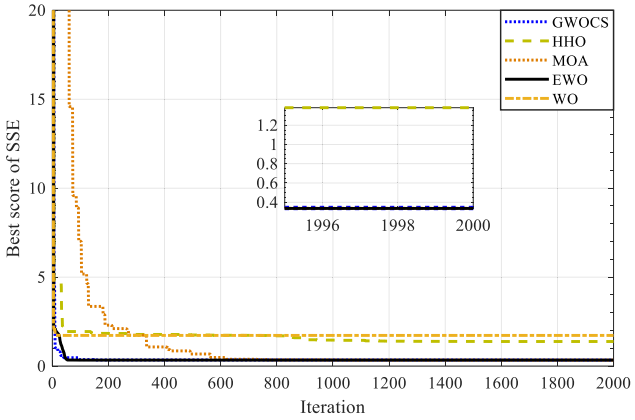

FIGURE 10. Convergence curves for case 2.

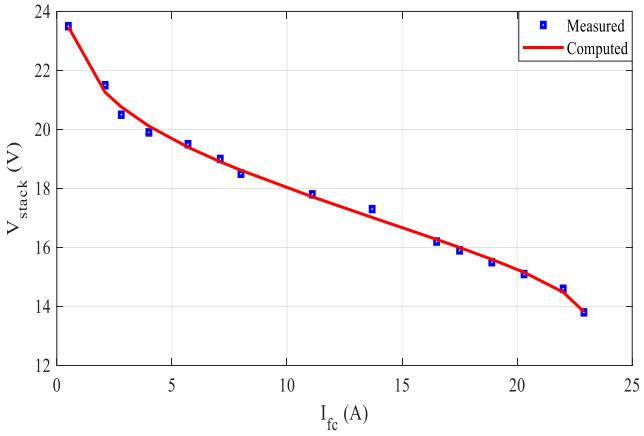

FIGURE 11. I-V curves for case 2.

pinpointing the results of the proposed EWO algorithm. This detailed part emphasizes the EWO's effectiveness in the optimization process, indicating its closer proximity to the optimal solution.

Figure 11 displays the I-V polarization characteristics for a 250W PEMFC stack, comparing measured data points with estimated values derived from an EWO model. A strong correlation between the calculated and measured values indicates

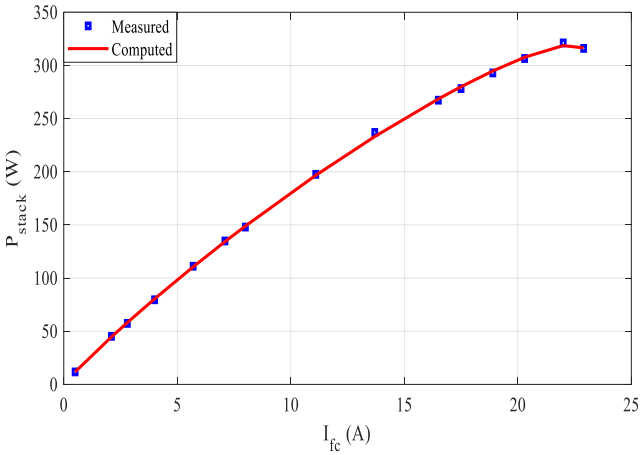

FIGURE 12. I-P curves for case 2.

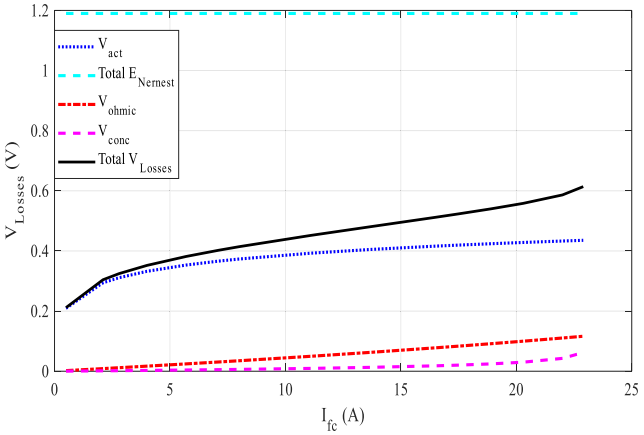

FIGURE 13. Graphical analysis of voltage losses for case 2.

an effective match between the observed values and the predictions of the EWO model. Similarly, Figure 12 presents the I-P curves for the same PEMFC stack. The graph demonstrates a strong correlation between the actual measurements and the estimated values, with the computed curve closely tracing the measured data points, thereby validating the model's accuracy in predicting the output power.

Figure 13 shows how various internal losses in a 250W PEMFC stack are related to the current. It offers a clear view of how the voltage losses in the PEMFC stack vary with the current.

The next two figures examine how a 250W PEMFC stack performs at different temperatures. Figure 14 shows a comparison of I-V curves at temperatures of 15, 40, and 60°C. The curves show that the voltage rises with temperature. At 60°C, the voltage remains higher across the current range compared to the voltage at 15°C and 40°C. Also, Figure 15 illustrates the comparison of I-P curves under the same temperature conditions. The output power shifts slightly as the temperature changes. The highest output power is observed at 60°C, and the lowest at 15°C.

Expanding on that, the simulations were performed at different pressures, keeping the temperature constant. The outcomes are graphically illustrated in Figure 16 and Figure 17.

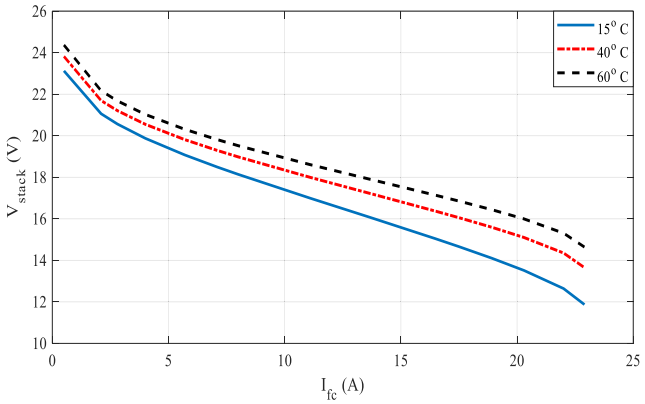

FIGURE 14. I-V curves at various temperatures for case 2.

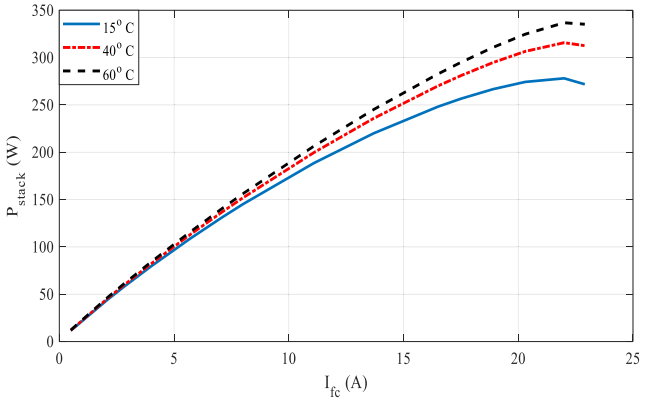

FIGURE 15. I-P curves at various temperatures for case 2.

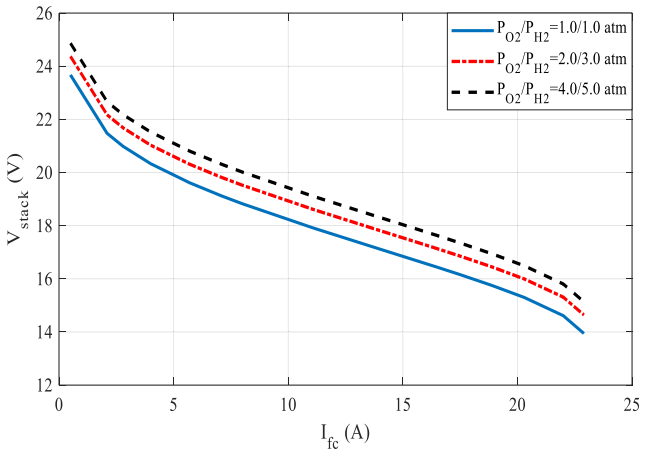

FIGURE 16. I-V curves at various pressures for case 2.

An evident rise in voltage is observed with increasing pressure. However. temperature variations influence the fuel cell's voltage and power output more obviously than pressure differences.

C. CASE 3: PERFORMANCE OF AVISTA SR-12 500 W PEMF

In this case, the AVISTA SR-12 500 W PEMFC stack, comprising 48 cells in series is evaluated for optimization against other algorithms. With an active area of 62.5 cm^2 besides a maximum current density of 0.672 A/cm^2, the PEMFC stack shows remarkable results. The optimization analysis

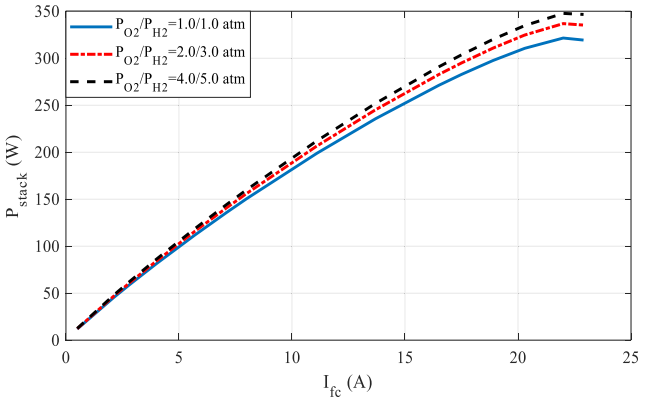

FIGURE 17. I-P curves at various pressures for case 2.

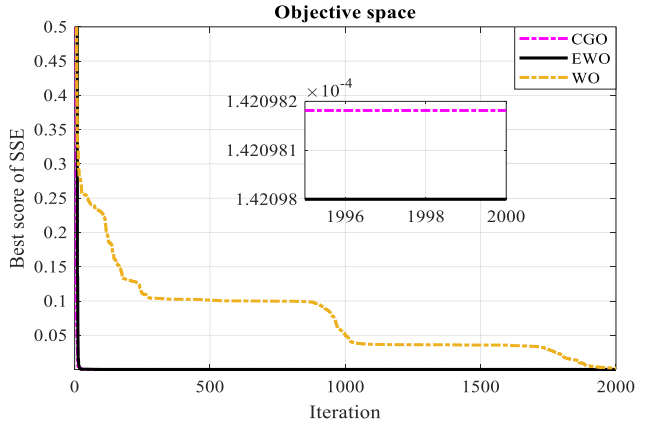

FIGURE 18. Convergence curves for case 3.

compared EWO with other known algorithms, namely chaos game optimization (CGO), neural network optimizer (NNO), and grasshopper optimizer (GHO).Table 3presents a comparison of the optimal values attained by the EWO with those acquired by other competing algorithms. The results for the EWO show a reduced SSE, indicating a higher level of optimization precision. Fig. 18 represents the trend of SSE minimization over iterations, featuring a magnified subfigure focusing on the outcomes of the EWO algorithm within the last five iterations. This detailed perspective sheds light on the performance of the EWO. Fig. 19 displays the current-voltage polarization characteristics of the AVISTA SR-12 500 W PEMFC, comparing measured data points with values predicted by an EWO model. A clear correlation exists between the predicted and measured values. Likewise, Fig. 20 presents the I-P curves for the same PEMFC, showing a visible link between the actual measurements and the estimated values.

Figure 21 illustrates the relationship between different internal losses within the AVISTA SR-12 500 W fuel cell and the current. It provides an overview of how the voltage losses within the PEMFC stack change with the current.

The upcoming two figures investigate the functioning characteristics of the AVISTA SR-12 500 W fuel cell stack at various temperatures. Fig. 22 compares I-V curves at temperatures of 15, 40, and 60°C. The curves show that the

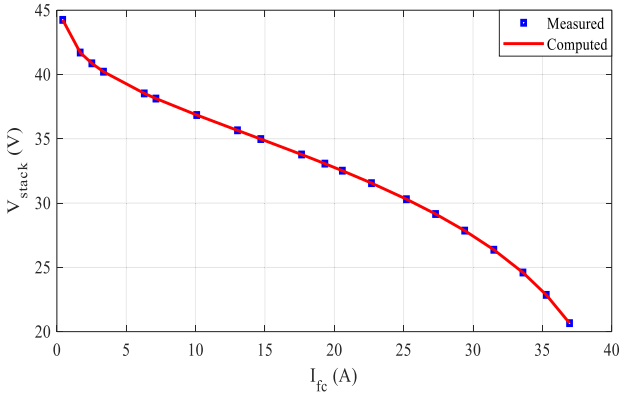

FIGURE 19. I-V curves for case 3.

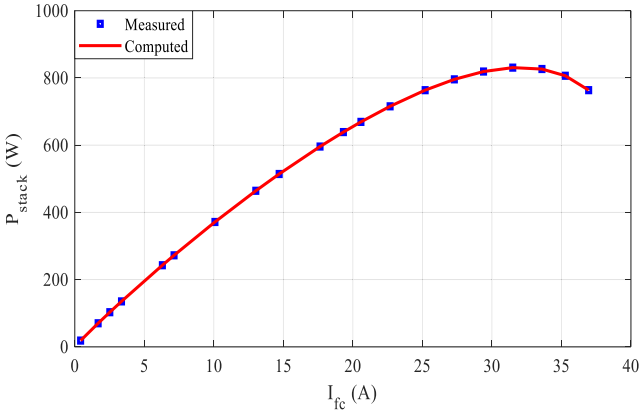

FIGURE 20. I-P curves for case 3.

TABLE 3. Design variables for case 3.

parameter	EWO	WO	CGO [38]	NNO [38]	GHO [38]
$\xi_1 \times 10^{-1}$	8.54148801	11.97349176	11.0531356	10.596	11.997
$\xi_2 \times 10^{-3}$	2.417998	4.194545	3.506655471	3.7435	4.2695
$\xi_3 \times 10^{-5}$	4.71474	9.3329	6.726482341	9.6902	9.8
$\xi_4 \times 10^{-5}$	-10.6347	-10.4969	-10.6347135	19.302	-10.1371
λ	21.51770845	22.999373 6	21.51771311	20.8772	23
$R_c \times 10^{-3}$	0.272639	0.395285	0.272639115	0.1	0.4638
β	0.150008477	0.1488775 9	0.150008476	0.0161	0.1486
SSE	0.000142	0.002004947	0.000142098	0.0117	0.0478

voltage rises with temperature. Also, Fig. 23 illustrates the comparison of I-P curves under the same temperature conditions. The output power shifts slightly as the temperature changes.

For this case, using the approaches used in prior cases, the simulations were done under various pressures at a constant temperature. The results are illustrated in Fig. 24 and Fig. 25. There is an increase in voltage as the pressure goes up.

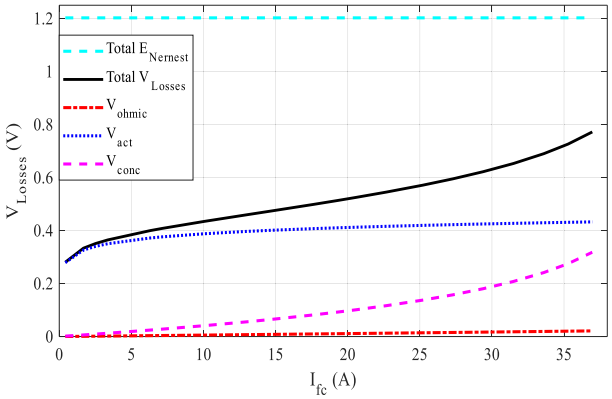

FIGURE 21. Graphical analysis of losses for case 3.

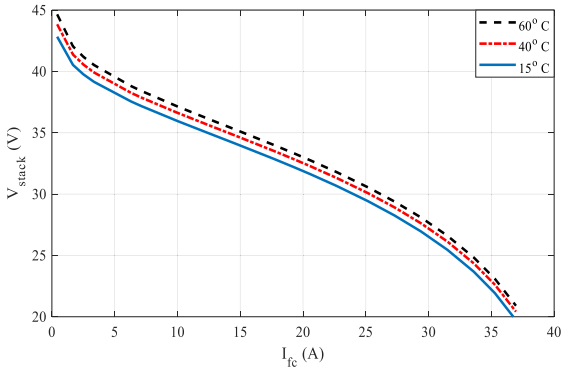

FIGURE 22. I-V curves at various temperatures for case 3.

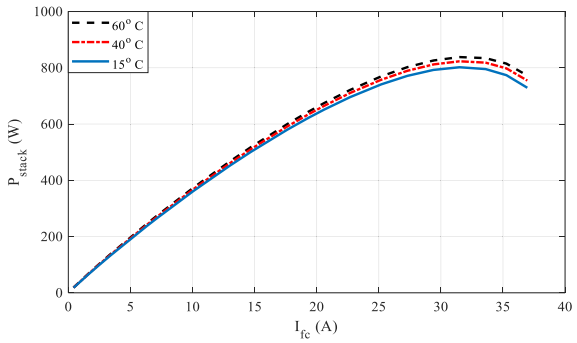

FIGURE 23. I-P curves at various temperatures for case 3.

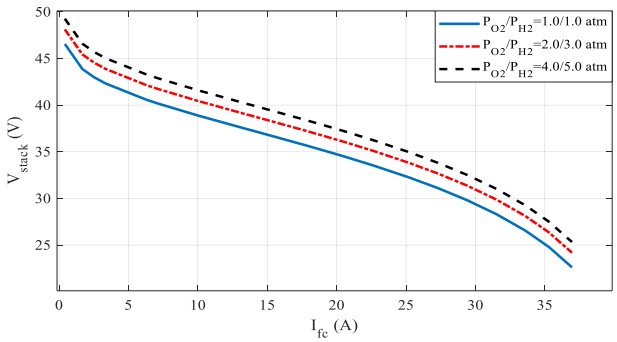

FIGURE 24. I-V curves at various pressures for Case 3.

D. CASE 4: PERFORMANCE OF TEMASEK 1 kW PEMF

With this case, the Temasek 1 kW PEM fuel cell, comprising 20 cells in series was evaluated for optimization in

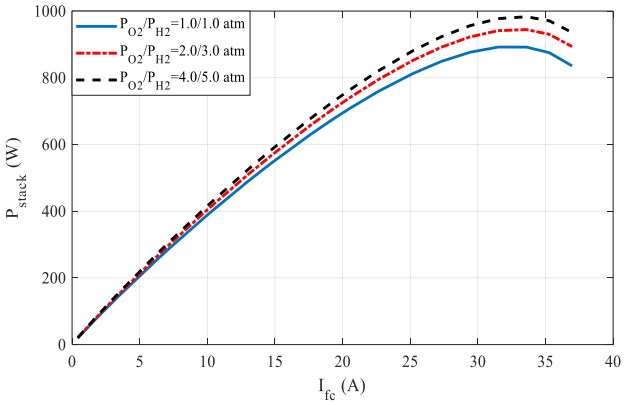

FIGURE 25. I-P curves at various pressures for case 3.

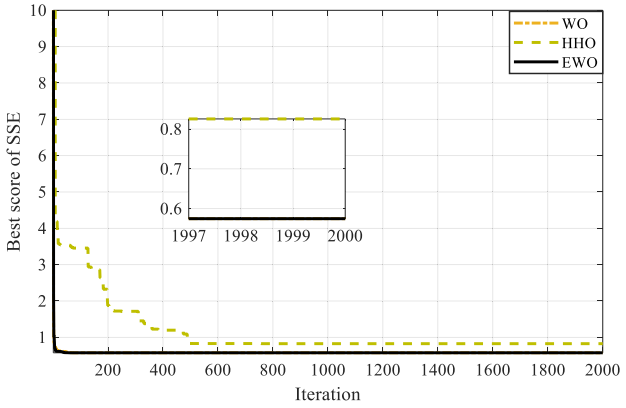

FIGURE 26. Convergence curves for case 4.

TABLE 4. Design variables for case 4.

parameter	EWO	WO	KOA [46]	MPA [46]	HHO [46]
$\xi_1 \times 10^{-1}$	-853200029	-8.813696	-8.731	-9.777	-8.532
$\xi_2 \times 10^{-3}$	2.364711	2.988173	2.7642	3.424	2.329774
$\xi_3 \times 10^{-5}$	3.77134	7.44626	6.1346	4.9692	3.6
$\xi_4 \times 10^{-5}$	-9.54	-9.54	-9.5	-23.6873	-9.54
λ	13	13	13	10	13
$R_c \times 10^{-3}$	0.1	0.1	0.1	0.1	0.8
β	0.163327328	0.163327329	0.1619	0.0225	0.0136
SSE	0.57476539	0.578753177	0.590467	0.7559	0.825511853

comparison with other algorithms. With an active area of 150 cm^2 and a maximum current density of 1.5 A/cm^2, the PEMFC stack shows remarkable results [46]. The optimization algorithms compared involve the kepler optimization algorithm (KOA), marine predator algorithm (MPA), and HHO. Table 4 enumerate the superior results achieved by the EWO against those obtained by the competing algorithms. The results for the EWO archive a lower SSE, suggesting refined accuracy in optimization. Fig. 26 represents the curve of SSE minimization across iterations.

Fig. 27 displays the current-voltage relationship for the Temasek 1 kW PEMFC, comparing measured data points with estimated values. There is a strong correlation between the calculated and measured values. Similarly, Fig. 28 presents the I-P curves for the same PEMFC.

Fig. 29 illustrates the relationship between different internal losses within the Temasek 1 kW PEM fuel cell and the

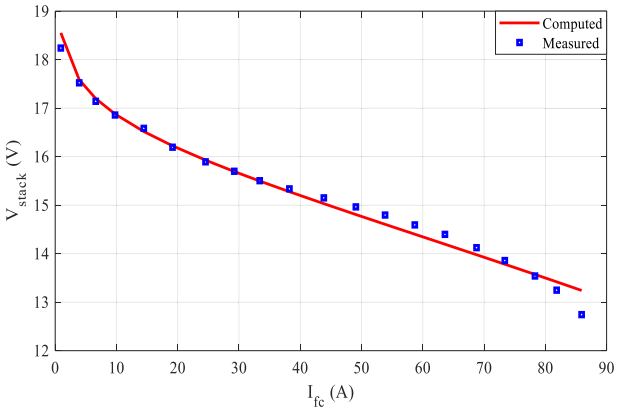

FIGURE 27. I-V curves for case 4.

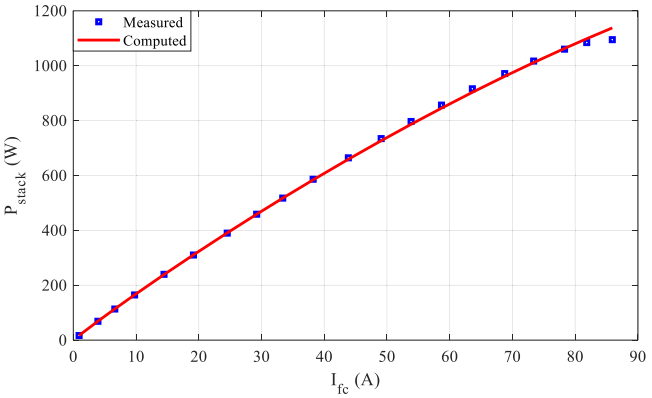

FIGURE 28. I-P curves for case 4.

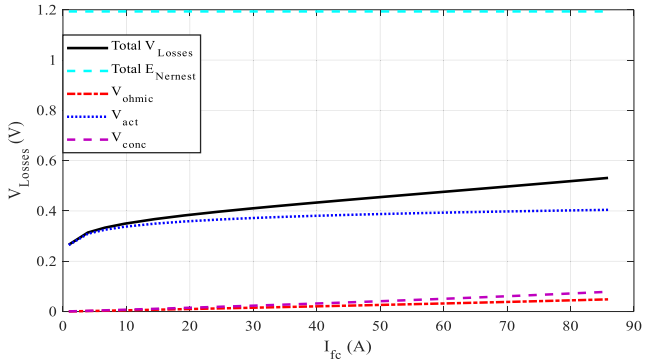

FIGURE 29. Graphical analysis of losses for case 4.

current. It offers an insight into the variation of voltage losses within the PEMFC stack as a function of current flow.

The following two figures investigate the performance characteristics of the Temasek 1 kW PEMFC stack at various temperatures. Fig. 30 shows a comparison of I-V curves at temperatures of 15, 40, and 60°C. Also, Fig. 31 illustrates the comparison of I-P curves under the same temperature conditions.

Consistent with previous testing conditions, the simulations were carried out at various pressures while maintaining a constant temperature. The results are depicted in Fig. 32 and Fig. 33.

The proposed EWO demonstrated its effectiveness by closely approximating the best results of the control variables

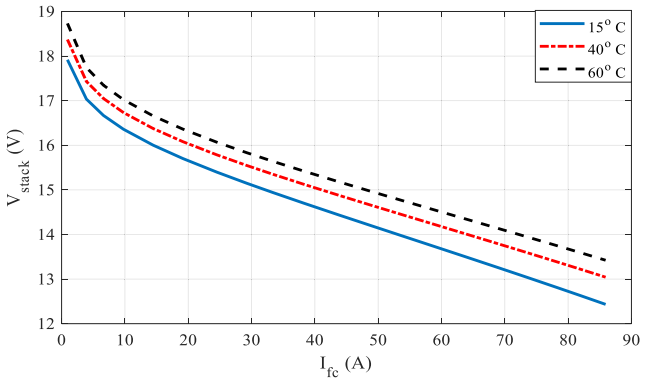

FIGURE 30. I-V curves at various temperatures for case 4.

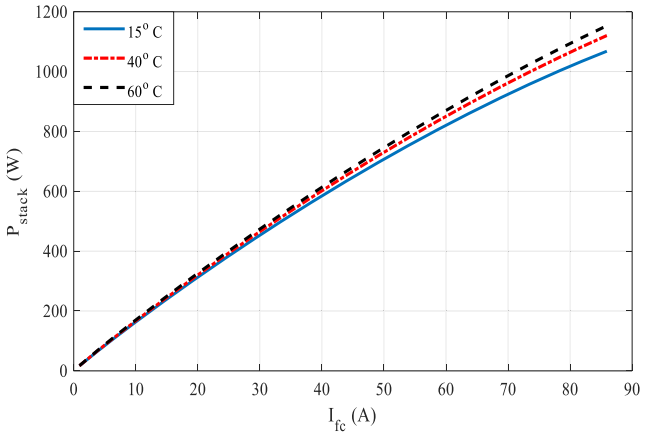

FIGURE 31. I-P curves at various temperatures for case 4.

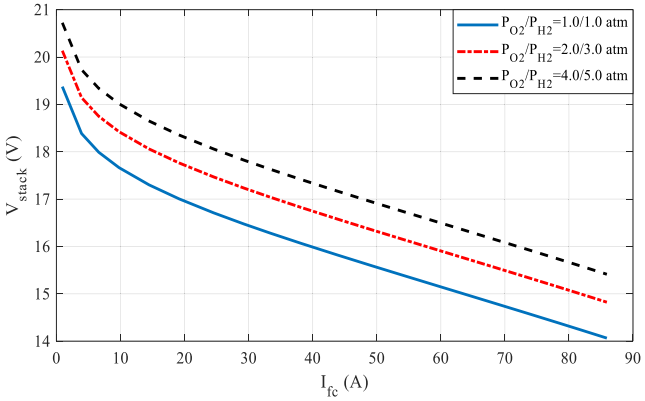

FIGURE 32. I-V curves at various pressures for case 4.

for the minimum SSE in PEMFCs. The performance of the EWO-based PEM fuel cell model highlights its superiority. This was further validated through a comparative analysis of experimental and theoretical simulation results. The deployment of the EWO has resulted in an accurate determination of the design variables for the PEMFC.

The parametric T-test is implemented to investigate the population characteristics. The T-test uses the results from 30 independent runs. Table 5 displays the detailed T-test outcomes for the four cases of the studied PEMFCs, presenting h-and p-values. These findings indicate that the EWO-based model is robust and demonstrates competitiveness.

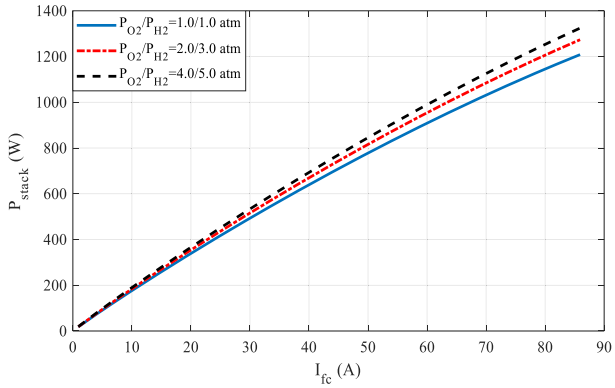

FIGURE 33. I-P curves at various pressures for case 4.

TABLE 5. Parametric test findings.

	Case 1	Case 2	Case 3	Case 4
h-values	0	0	0	0
p-values	0.99987	1	1	1
Degree of freedom	499	499	499	199
Standard deviation	0.000088	0.718301	0.04741	0.000282

VI. CONCLUSION

In conclusion, this article introduces an innovative method for accurately estimating parameters in PEMFC models through the use of an Enhanced WO algorithm. The goal is to develop a reliable theoretical model for PEMFCs that aligns closely with experimental data, thereby advancing optimization techniques in fuel cell research. The work emphasizes the importance of precise PEMFC modeling, addresses the complexities of modeling nonlinear systems, and highlights the necessity for better optimization methods. The EWO algorithm, introduced here, shows superior capability in optimizing the fitness function. A mathematical model of the PEMFC is presented, detailing essential parameters like activation overpotential, resistance voltage loss, and concentration overpotential. This model was tested under various pressures and temperatures, with simulated current-voltage (I-V) curves compared to experimental data across four test scenarios. In the 6 kW Nedstack PS6 scenario, the EWO successfully improved terminal voltage, demonstrating its ability to fine-tune the design variables. In the AVISTA SR-12 500 W scenario, the optimizer minimized the SSE, highlighting its efficiency optimization potential. The investigation of the 250W stack further confirmed EWO's efficiency, and the Temasek 1 kW case offered insights into the algorithm's smooth and speed convergence. Future research directions may include further enhancements to the modeling approach and exploring additional optimization algorithms for PEMFC parameters estimation.

ACKNOWLEDGMENT

This work was supported by the Researchers Supporting Project number (RSP2024R467), King Saud University, Riyadh, Saudi Arabia.

REFERENCES

[1] G. Mutezo and J. Mulopo, "A review of Africa's transition from fossil fuels to renewable energy using circular economy principles," *Renew. Sustain. Energy Rev.*, vol. 137, Mar. 2021, Art. no. 110609, doi: 10.1016/j.rser.2020.110609.

[2] K. Obileke, H. Onyeaka, E. L. Meyer, and N. Nwokolo, "Microbial fuel cells, a renewable energy technology for bio-electricity generation: A mini-review," *Electrochemistry Commun.*, vol. 125, Apr. 2021, Art. no. 107003, doi: 10.1016/j.elecom.2021.107003.

[3] M. A. Abdelkareem, K. Elsaid, T. Wilberforce, M. Kamil, E. T. Sayed, and A. Olabi, "Environmental aspects of fuel cells: A review," *Sci. Total Environ.*, vol. 752, Jan. 2021, Art. no. 141803, doi: 10.1016/j.scitotenv.2020.141803.

[4] Z. Huang, L. Xing, and Z. Tu, "Load changing characteristics of the hydrogen-air and hydrogen-oxygen proton exchange membrane fuel cells," *Int. J. Energy Res.*, vol. 46, no. 2, pp. 1909–1921, Feb. 2022, doi: 10.1002/er.7306.

[5] K. Meng, B. Chen, H. Zhou, J. Shen, Z. Shen, and Z. Tu, "Investigation on degradation mechanism of hydrogen–oxygen proton exchange membrane fuel cell under current cyclic loading," *Energy*, vol. 242, Mar. 2022, Art. no. 123045, doi: 10.1016/j.energy.2021.123045.

[6] D. Çalışır, S. Ekici, A. Midilli, and T. H. Karakoc, "Benchmarking environmental impacts of power groups used in a designed UAV: Hybrid hydrogen fuel cell system versus lithium-polymer battery drive system," *Energy*, vol. 262, Jan. 2023, Art. no. 125543, doi: 10.1016/j.energy.2022.125543.

[7] E. Qu, X. Hao, M. Xiao, D. Han, S. Huang, Z. Huang, S. Wang, and Y. Meng, "Proton exchange membranes for high temperature proton exchange membrane fuel cells: Challenges and perspectives," *J. Power Sources*, vol. 533, Jun. 2022, Art. no. 231386, doi: 10.1016/j.jpowsour.2022.231386.

[8] Q. Xu, Z. Guo, L. Xia, Q. He, Z. Li, I. T. Bello, K. Zheng, and M. Ni, "A comprehensive review of solid oxide fuel cells operating on various promising alternative fuels," *Energy Convers. Manage.*, vol. 253, Feb. 2022, Art. no. 115175, doi: 10.1016/j.enconman.2021.115175.

[9] S. Samanta and D. Roy, "Molten carbonate fuel cell integrated hybrid system for clean and efficient power generation," *Appl. Thermal Eng.*, vol. 226, May 2023, Art. no. 120294, doi: 10.1016/j.applthermaleng.2023.120294.

[10] O. Corigliano, L. Pagnotta, and P. Fragiacomo, "On the technology of solid oxide fuel cell (SOFC) energy systems for stationary power generation: A review," *Sustainability*, vol. 14, no. 22, p. 15276, Nov. 2022, doi: 10.3390/su142215276.

[11] D. A. Jadhav, S.-G. Park, T. Eisa, A. K. Mungray, E. C. Madenli, A.-G. Olabi, M. A. Abdelkareem, and K.-J. Chae, "Current outlook towards feasibility and sustainability of ceramic membranes for practical scalable applications of microbial fuel cells," *Renew. Sustain. Energy Rev.*, vol. 167, Oct. 2022, Art. no. 112769, doi: 10.1016/j.rser.2022.112769.

[12] A. G. Elkafas, M. Rivarolo, E. Gadducci, L. Magistri, and A. F. Massardo, "Fuel cell systems for maritime: A review of research development, commercial products, applications, and perspectives," *Processes*, vol. 11, no. 1, p. 97, Dec. 2022, doi: 10.3390/pr11010097.

[13] X. Chen, S. Long, L. He, C. Wang, F. Chai, X. Kong, Z. Wan, X. Song, and Z. Tu, "Performance evaluation on thermodynamics-economy-environment of PEMFC vehicle power system under dynamic condition," *Energy Convers. Manage.*, vol. 269, Oct. 2022, Art. no. 116082, doi: 10.1016/j.enconman.2022.116082.

[14] L. Fan, Z. Tu, and S. H. Chan, "Recent development of hydrogen and fuel cell technologies: A review," *Energy Rep.*, vol. 7, pp. 8421–8446, Nov. 2021, doi: 10.1016/j.egyr.2021.08.003.

[15] M. A. Aminudin, S. K. Kamarudin, B. H. Lim, E. H. Majilan, M. S. Masdar, and N. Shaari, "An overview: Current progress on hydrogen fuel cell vehicles," *Int. J. Hydrogen Energy*, vol. 48, no. 11, pp. 4371–4388, Feb. 2023, doi: 10.1016/j.ijhydene.2022.10.156.

[16] A. M. Hussien, H. M. Hasanien, and S. F. Mekhamer, "Sunflower optimization algorithm-based optimal PI control for enhancing the performance of an autonomous operation of a microgrid," *Ain Shams Eng. J.*, vol. 12, no. 2, pp. 1883–1893, Jun. 2021, doi: 10.1016/j.asej.2020.10.020.

[17] K. Meng, B. Chen, H. Zhou, J. Shen, and Z. Tu, "Experimental investigation on voltage response characteristics of hydrogen-oxygen proton exchange membrane fuel cells under gas starvation," *Energy Convers. Manage.*, vol. 268, Sep. 2022, Art. no. 115973, doi: 10.1016/j.enconman.2022.115973.

[18] S. A. Korkmaz, S. A. Çetinkaya, O. Yuksel, O. Konur, K. E. Erginer, and C. O. Colpan, "Comparison of various metaheuristic algorithms to extract the optimal PEMFC modeling parameters," *Int. J. Hydrogen Energy*, vol. 51, pp. 1402–1420, Jan. 2024, doi: 10.1016/j.ijhydene.2023.05.347.

[19] B. Kanouni, A. E. Badoud, and S. Mekhilef, "A multi-objective model predictive current control with two-step horizon for double-stage grid-connected inverter PEMFC system," *Int. J. Hydrogen Energy*, vol. 47, no. 4, pp. 2685–2707, Jan. 2022, doi: 10.1016/j.ijhydene.2021.10.182.

[20] X. Zhao, Y. Zhou, L. Wang, B. Pan, R. Wang, and L. Wang, "Classification, summarization and perspective on modeling techniques for polymer electrolyte membrane fuel cell," *Int. J. Hydrogen Energy*, vol. 48, no. 57, pp. 21864–21885, Jul. 2023, doi: 10.1016/j.ijhydene.2023.03.033.

[21] A. M. Hussien, R. A. Turky, A. Alkuhayli, H. M. Hasanien, M. Tostado-Véiz, F. Jurado, and R. C. Bansal, "Coot bird algorithms-based tuning PI controller for optimal microgrid autonomous operation," *IEEE Access*, vol. 10, pp. 6442–6458, 2022, doi: 10.1109/ACCESS.2022.3142742.

[22] Y. Chen, D. Pi, B. Wang, J. Chen, and Y. Xu, "Bi-subgroup optimization algorithm for parameter estimation of a PEMFC model," *Expert Syst. Appl.*, vol. 196, Jun. 2022, Art. no. 116646, doi: 10.1016/j.eswa.2022.116646.

[23] H. Ashraf, S. O. Abdellatif, M. M. Elkholy, and A. A. El-Fergany, "Computational techniques based on artificial intelligence for extracting optimal parameters of PEMFCs: Survey and insights," *Arch. Comput. Methods Eng.*, vol. 29, no. 6, pp. 3943–3972, Oct. 2022, doi: 10.1007/s11831-022-09721-y.

[24] U. Mitra, A. Arya, and S. Gupta, "A comprehensive and comparative review on parameter estimation methods for modelling proton exchange membrane fuel cell," *Fuel*, vol. 335, Mar. 2023, Art. no. 127080, doi: 10.1016/j.fuel.2022.127080.

[25] M. Ćalasan, M. Micev, H. M. Hasanien, and S. H. E. A. Aleem, "PEM fuel cells: Two novel approaches for mathematical modeling and parameter estimation," *Energy*, vol. 290, Mar. 2024, Art. no. 130130, doi: 10.1016/j.energy.2023.130130.

[26] H. Zhou, X. Wu, Y. Li, Z. Fan, W. Chen, J. Mao, P. Deng, and T. Wik, "Model optimization of a high-power commercial PEMFC system via an improved grey wolf optimization method," *Fuel*, vol. 357, Feb. 2024, Art. no. 129589, doi: 10.1016/j.fuel.2023.129589.

[27] Y. Zhao, M. Luo, J. Yang, B. Chen, and P.-C. Sui, "Numerical analysis of PEMFC stack performance degradation using an empirical approach," *Int. J. Hydrogen Energy*, vol. 56, pp. 147–163, Feb. 2024, doi: 10.1016/j.ijhydene.2023.12.096.

[28] A. A. Z. Diab and A. M. Abdelhamid, "Optimal identification of model parameters for PEMFCs using neoteric metaheuristic methods," *IET Renew. Power Gener.*, vol. 17, no. 3, pp. 659–680, Feb. 2023, doi: 10.1049/rpg2.12621.

[29] H. M. Sultan, A. S. Menesy, M. Alqahtani, M. Khalid, and A. A. Z. Diab, "Accurate parameter identification of proton exchange membrane fuel cell models using different metaheuristic optimization algorithms," *Energy Rep.*, vol. 10, pp. 4824–4848, Nov. 2023, doi: 10.1016/j.egyr.2023.11.007.

[30] X. Liu, Y. Yang, L. Zhang, S. Zhou, L. Xu, C. Xie, B. Zhao, and L. Zhang, "Uncertainty assessment of a semi-empirical output voltage model for proton exchange membrane fuel cells," *Int. J. Hydrogen Energy*, vol. 48, no. 29, pp. 11071–11085, Apr. 2023, doi: 10.1016/j.ijhydene.2022.12.106.

[31] Y. Wang, K. Wu, H. Zhao, J. Li, X. Sheng, Y. Yin, Q. Du, B. Zu, L. Han, and K. Jiao, "Degradation prediction of proton exchange membrane fuel cell stack using semi-empirical and data-driven methods," *Energy AI*, vol. 11, Jan. 2023, Art. no. 100205, doi: 10.1016/j.egyai.2022.100205.

[32] A. Abbou, A. El Hasnaoui, S. S. Khan, and F. Yamin, "Analysis of the novel dynamic semiempirical model of proton exchange membrane fuel cell by incorporating ambient condition variations," *Int. J. Energy Environ. Eng.*, vol. 13, no. 1, pp. 105–120, Mar. 2022, doi: 10.1007/s40095-021-00410-3.

[33] K. Yuan, Y. Ma, H. Zhang, N. Razmjooy, and N. Ghadimi, "Optimal parameters estimation of the proton exchange membrane fuel cell stacks using a combined owl search algorithm," *Energy Sources A, Recovery, Utilization, Environ. Effects*, vol. 45, no. 4, pp. 11712–11732, Oct. 2023, doi: 10.1080/15567036.2023.2252672.

[34] R. Abbassi, S. Saidi, A. Abbassi, H. Jerbi, M. Kchaou, and B. N. Alhasnawi, "Accurate key parameters estimation of PEMFCs' models based on dandelion optimization algorithm," *Mathematics*, vol. 11, no. 6, p. 1298, Mar. 2023, doi: 10.3390/math11061298.

[35] X. Bao, H. Jia, and C. Lang, "A novel hybrid Harris hawks optimization for color image multilevel thresholding segmentation," *IEEE Access*, vol. 7, pp. 76529–76546, 2019, doi: 10.1109/ACCESS.2019.2921545.
[36] H. M. Hasanien, M. A. M. Shaheen, R. A. Turky, M. H. Qais, S. Alghuwainem, S. Kamel, M. Tostado-Véliz, and F. Jurado, "Precise modeling of PEM fuel cell using a novel enhanced transient search optimization algorithm," *Energy*, vol. 247, May 2022, Art. no. 123530, doi: 10.1016/j.energy.2022.123530.
[37] I. Alsaidan, M. A. M. Shaheen, H. M. Hasanien, M. Alaraj, and A. S. Alnafisah, "Proton exchange membrane fuel cells modeling using chaos game optimization technique," *Sustainability*, vol. 13, no. 14, p. 7911, Jul. 2021, doi: 10.3390/su13147911.
[38] I. Alsaidan, M. A. M. Shaheen, H. M. Hasanien, M. Alaraj, and A. S. Alnafisah, "A PEMFC model optimization using the enhanced bald eagle algorithm," *Ain Shams Eng. J.*, vol. 13, no. 6, Nov. 2022, Art. no. 101749, doi: 10.1016/j.asej.2022.101749.
[39] S. I. Selem, H. M. Hasanien, and A. A. El-Fergany, "Parameters extraction of PEMFC's model using manta rays foraging optimizer," *Int. J. Energy Res.*, vol. 44, no. 6, pp. 4629–4640, May 2020, doi: 10.1002/er.5244.
[40] M. A. M. Shaheen, H. M. Hasanien, M. S. El Moursi, and A. A. El-Fergany, "Precise modeling of PEM fuel cell using improved chaotic MayFly optimization algorithm," *Int. J. Energy Res.*, vol. 45, no. 13, pp. 18754–18769, Oct. 2021, doi: 10.1002/er.6987.
[41] M. Han, Z. Du, K. F. Yuen, H. Zhu, Y. Li, and Q. Yuan, "Walrus optimizer: A novel nature-inspired metaheuristic algorithm," *Expert Syst. Appl.*, vol. 239, Apr. 2024, Art. no. 122413, doi: 10.1016/j.eswa.2023.122413.
[42] J. Li, Q. An, H. Lei, Q. Deng, and G.-G. Wang, "Survey of Lévy flight-based metaheuristics for optimization," *Mathematics*, vol. 10, no. 15, p. 2785, Aug. 2022, doi: 10.3390/math10152785.
[43] G. Iacca, V. C. dos Santos Junior, and V. V. de Melo, "An improved Jaya optimization algorithm with Lévy flight," *Expert Syst. Appl.*, vol. 165, Mar. 2021, Art. no. 113902, doi: 10.1016/j.eswa.2020.113902.
[44] M. H. Hassan, S. Kamel, F. Jurado, M. Ebeed, and M. F. Elnaggar, "Economic load dispatch solution of large-scale power systems using an enhanced Beluga whale optimizer," *Alexandria Eng. J.*, vol. 72, pp. 573–591, Jun. 2023, doi: 10.1016/j.aej.2023.04.002.
[45] M. A. M. Shaheen, Z. Ullah, H. M. Hasanien, M. Tostado-Véliz, H. Ji, M. H. Qais, S. Alghuwainem, and F. Jurado, "Enhanced transient search optimization algorithm-based optimal reactive power dispatch including electric vehicles," *Energy*, vol. 277, Aug. 2023, Art. no. 127711, doi: 10.1016/j.energy.2023.127711.
[46] H. Ashraf, M. M. Elkholy, S. O. Abdellatif, and A. A. El-Fergany, "Accurate emulation of steady-state and dynamic performances of PEM fuel cells using simplified models," *Sci. Rep.*, vol. 13, no. 1, pp. 1–18, Nov. 2023, doi: 10.1038/s41598-023-46847-w.

AYEDH H. ALQAHTANI (Senior Member, IEEE) received the B.Sc. degree in electrical engineering from The University of North Carolina at Charlotte, Charlotte, NC, USA, in 2000, the M.Sc. degree from the University of Southern California, Los Angeles, CA, USA, in 2005, and the Ph.D. degree in electrical engineering from The Ohio State University, Columbus, OH, USA, in 2013. His current research interests include the integration of renewable energy into electric power systems, modeling and control of distributed energy generation, and the development of green-energy systems. His contributions to the field are geared toward enhancing the sustainability and efficiency of energy systems.

HANY M. HASANIEN (Senior Member, IEEE) received the B.Sc., M.Sc., and Ph.D. degrees in electrical engineering from the Faculty of Engineering, Ain Shams University, Cairo, Egypt, in 1999, 2004, and 2007, respectively. From 2008 to 2011, he was a Joint Researcher with Kitami Institute of Technology, Kitami, Japan. From 2011 to 2015, he was an Associate Professor with the College of Engineering, King Saud University, Riyadh, Saudi Arabia. He is currently a Professor with the Electrical Power and Machines Department, Faculty of Engineering, Ain Shams University. He has authored, coauthored, and edited three books in the field of electric machines and renewable energy. He has published more than 290 papers in international journals and conferences. His research interests include modern control techniques, power systems dynamics and control, energy storage systems, renewable energy systems, and smart grid. He is an Editorial Board Member of *Electric Power Components and Systems*. His biography has been included in Marquis Who's Who in the World for its 28 Edition, in 2011. He was awarded the Encouraging Egypt Award for Engineering Sciences in 2012, the Institutions Egypt Award for Invention and Innovation of Renewable Energy Systems Development in 2014, the Superiority Egypt Award for Engineering Sciences in 2019, and the Ain Shams University Appreciation Award in Engineering Sciences for 2022. He was the IEEE PES Egypt Chapter Chair (2020–2022). He is the Subject Editor of *IET Renewable Power Generation*, *Frontiers in Energy Research*, and *Electronics* (MDPI). He is the Editor-in-Chief of *Ain Shams Engineering Journal* (Elsevier).

MOHAMMED ALHARBI received the B.S. degree in electrical engineering from King Saud University, Riyadh, Saudi Arabia, in 2010, the M.S. degree in electrical engineering from Missouri University of Science and Technology, Rolla, MO, USA, in 2014, and the Ph.D. degree in electrical engineering from North Carolina State University, Raleigh, NC, USA, in 2020. He was a Teaching Assistant with King Saud University, from September 2010 to May 2011. He was a Project Engineer with the FREEDM Systems Center, North Carolina State University, from January 2016 to December 2019, where he was involved in designing and constructing a modular multi-level converter for control validations. In August 2020, he joined the Department of Electrical Engineering, King Saud University, where he is currently an Assistant Professor. His research interests include medium voltage and high-power converters, modular multi-level converter (MMC) controls, multi-terminal HVdc systems, and grid integration of renewable energy systems.

SUN CHUANYU (Member, IEEE) received he bachelor's degree from Tianjin University, in 2012, the master's degree from Politecnico di Milano, in 2014, and the Ph.D. degree from Università degli Studi di Padova, in 2019. He has been an Associate Professor with the School of Electrical Engineering and Automation, Harbin Institute of Technology, since October 2022. His current research interests include fuel cells and redox flow batteries for large-scale energy storage applications, as well as their design, optimization, and modeling study.